RSC Advances

PAPER

Cite this: *RSC Adv.*, 2019, **9**, 30432

Assembly with copper(II) ions and D–π–A molecules on a graphene surface for ultra-fast acetic acid sensing at room temperature†

Yelei Gong,‡[a] Hao Li,‡[a] Wenle Pei,[b] Jincheng Fan,[a] Ahmad Umar,[c] M. S. Al-Assiri,[cd] Yao Wang,*[a] Nicolaas Frans de Rooij[a] and Guofu Zhou[a]

In this study, a graphene-based composite 4HQ-rGO/Cu^{2+} was prepared *via* the supramolecular assembly of graphene nanosheets with 4-hydroxyquinoline (4HQ) and copper(II) ions. The as-prepared supramolecular assembly exhibited an excellent and enhanced sensing performance towards acetic acid at room-temperature, which was due to the fact that the D–π–A molecules, *i.e.* 4HQ, were able to accelerate the charge transfer between the graphene nanosheets and 4HQ molecules when acetic acid was attached. In addition, at room temperature, the copper(II) ions also played a critical role as the main active site for gas adsorption, and thus the as-fabricated sensor exhibited a high response, outstanding selectivity, and ultra-fast response/recovery time. To examine the selectivity of the Cu^{2+} ions for the supramolecular assembly, various other transition metal ions such as Mn^{2+}, Fe^{3+}, Co^{2+}, Ni^{2+}, Cu^{2+}, and Cd^{2+} were attached to the 4HQ-rGO assembly, and their acetic sensing performance was determined. Interestingly, the supramolecular assembly with the Cu^{2+} ions (4HQ-rGO/Cu^{2+}) exhibited the best sensing performance compared to other metal ion-based 4HQ-rGO materials. Compared with the typical acetic acid gas sensors reported in the literature, it is noteworthy to mention that the as-prepared 4HQ-rGO/Cu^{2+} supramolecular assembly exhibited the shortest gas response time (within 5 s) at room temperature. The presented study demonstrates that the as-prepared supramolecular assembly is a promising material as a room temperature acetic acid gas sensor in practical applications.

Received 23rd July 2019
Accepted 11th September 2019

DOI: 10.1039/c9ra05706d

rsc.li/rsc-advances

1. Introduction

Acetic acid is one of the volatile organic compounds (VOCs) that is broadly used in dyes, manufacturing, photographic chemicals, and food industries.[1,2] Even though it is widely used, a prolonged exposure to high concentrations of acetic acid may cause severe health hazards, such as skin irritation, body swelling, particularly on the tongue, throat, lips, face, *etc.*, and grim breathing.[2,3] Thus, developing an ultrasensitive, low-energy consuming, and reliable acetic acid gas sensor is quite important for air monitoring in modern industries. As reported, micro- and nano-metric gas sensors based on metal-oxides exhibit excellent sensing performances at certain relatively high working temperatures although poor selectivity and high energy consumption are still a concern in research for practical applications.[3–6] Nowadays, it is still a challenge to manufacture a room-temperature gas sensor that has an excellent response to acetic acid with good selectivity and short response and recovery times.

In the past few years, graphene-based gas sensing materials have attracted considerable interest because of numerous advantages, such as a high response, short response time, low detection limit, and low working temperature (*i.e.*, room-temperature).[7–9] In addition, the distinctive morphology of graphene endues a sensitive response to small changes in an ambient environment, and the functionalization of graphene nanosheets with various "guests" (*i.e.*, organic molecules and nanoparticles) offers a unique selectivity for the resultant gas sensors.[10–13] It is known that the supramolecular assembly of graphene would retain the inherent structure of graphene and construct a better functional gas sensing scaffold.[14–17] For example, molecules with a D–π–A structure have the ability to notably improve gas sensing characteristics by enhancing the charge transfer between graphene and the assembled molecules.[15] Moreover, the supramolecular assembly of graphene with "guests" can be easily conducted under mild conditions, showing promise

[a]*Guangdong Provincial Key Laboratory of Optical Information Materials and Technology, Institute of Electronic Paper Displays, South China Academy of Advanced Optoelectronics, South China Normal University, Guangzhou 510006, P. R. China. E-mail: wangyao@m.scnu.edu.cn*

[b]*Key Laboratory of Bio-Inspired Smart Interfacial Science and Technology of Ministry of Education, School of Chemistry, Beihang University, Beijing 100191, P. R. China*

[c]*Promising Centre for Sensors and Electronic Devices, Najran University, Najran 11001, Kingdom of Saudi Arabia*

[d]*Department of Chemistry, Faculty of Science and Arts, Najran University, Najran-11001, Saudi Arabia*

† Electronic supplementary information (ESI) available. See DOI: 10.1039/c9ra05706d

‡ These authors contributed equally to this work.

for preparing commercial gas sensors.[18] So far, only a few studies on graphene-based acetic acid sensors have been reported.[19–22]

As stated above, it is important to find a protocol to decrease the working temperature of the gas sensors. It is known that many transition metals, such as V, Fe, Cr, and Cu, show good catalytic properties under a low temperature,[23–27] which implies the possibility of enhancing the charge transfer at low temperatures during the gas sensing process. Among those transition metal ions, copper is a typically widely used catalyst in the selective catalytic reduction reactions because the existence of the d-electron density of the copper ion (Cu^{2+}) active sites promotes charge transfer inside the material.[24,25] Hence, we have a reason to propose that the presence of Cu^{2+} would also promote the charge transfer process inside the graphene-based composite, thereby improving the room temperature gas sensing characteristics.

In this study, we report a graphene-based sensing composite with an excellent comprehensive performance. 4HQ-rGO/Cu^{2+} was fabricated *via* the supramolecular assembly of graphene nanosheets with 4-hydroxyquinoline and the electrostatic adsorption of copper(II) ion. The room-temperature acetic acid sensing performance of the as-prepared composite was systematically investigated. The results revealed that the 4HQ-rGO/Cu^{2+}-based acetic acid gas sensor exhibited outstanding selectivity, high sensitivity, and ultra-fast response/recovery (response and recovery times of 5 s each).

2. Experimental section

2.1 Preparation of GO, rGO, 4HQ-rGO and 4HQ-rGO/Cu^{2+} materials

GO flakes (procured from XianFeng NANO Co, Ltd.) were dispersed in deionized (DI) water *via* a 1 h sonication process in order to obtain a 1 mg mL^{-1} homogeneous suspension. The rGO suspension was prepared by diluting 4 mL the GO suspension (1 mg mL^{-1}) with 16 mL DI water. Then, as a reductant, 100 μL of ammonia (30%) and 10 mL of hydrazine hydrate (1.12 μL mL^{-1}) were successively dropped into the above suspension under stirring. The mixture was placed in an oil bath (85 °C) and heated for 1 h. The color change of the solution from brownish yellow to black proved the conversion of GO to rGO. To prepare the 4HQ-rGO dispersion, 90 mg of 4HQ (purchased from Alfa Aesar), 10 mL DI water, 4 mL the GO suspension, and 0.1 mL ammonia (30%) were mixed to yield a homogeneous mixture. After adding 10 mL hydrazine hydrate under stirring, the mixture was heated at 85 °C for 1 h. Finally, the resultant solution was washed with DI water for few times using vacuum filtration, and the obtained slurry was again re-dispersed in DI water (20 mL) under mild sonication. The $CuCl_2$ aqueous solution (0.5 mL) with different Cu^{2+} contents was subsequently added to form a series of the 4HQ-rGO/Cu^{2+} suspension with Cu^{2+} concentrations of 5, 10, 15, 20, and 50 mg mL^{-1}.

2.2 Fabrication of rGO, 4HQ-rGO and 4HQ-rGO/Cu^{2+} based gas sensors

Interdigitated electrodes (IDEs) were washed sequentially using DI water and acetone for 20 min under gentle sonication. The as-prepared solution was dropped on the IDEs to fabricate all the sensors, followed by a drying process. To fabricate the IDEs, Ag–Pd paste was jetted onto the ceramic plates *via* a metal-jetting system (10 digits with 5 μm fingers and 15 μm gaps, Synkera). Briefly, 30 μL rGO, 4HQ-rGO, and 4HQ-rGO/Cu^{2+} suspension (0.2 mg mL^{-1}) were assembled on the surface of the IDEs. Finally, the gas sensors were obtained after drying the coated IDEs naturally.

2.3 Characterizations

The characterization of the general structures for the as-prepared samples was measured by field emission scanning electron microscopy (FESEM; Quanta 250 FEG, FEI). The surface structural properties were analyzed by Raman-scattering spectroscopy (HORIBA Jobin Yvon Raman microscope, LabRAM HR800) with a 647 nm laser line as the exciton source. The chemical compositions of the materials were examined by fourier transform infrared (FTIR; NicoletiN10MX) spectroscopy and X-ray photoelectron spectroscopy (XPS; ESCALAB250 photoelectron spectrometer, Thermo Fisher Scientific, USA).

2.4 Gas sensing measurements

To check the gas sensing characteristics, a CGS-1TP, ELITE TECH intelligent gas sensing system was used. The resistance variations for the as-prepared sensors were automatically detected by the system (resistance measurement range: 0 Ω to 2 GΩ). Ambient air gas was aerated into two glass gas cylinders before the gas sensing measurements. Then, a quantitative acetic acid solution was injected into one of them and diffused evenly. The sensor response was defined as $|R_a - R_g|/R_a \times 100\%$, where R_a and R_g are the resistances of the sensing material recorded in air and the acetic acid atmosphere, respectively. Due to the ultrafast response and recovery rate, the response time was defined as the time taken for the sensor to reach its steady value. The recovery time was the time required

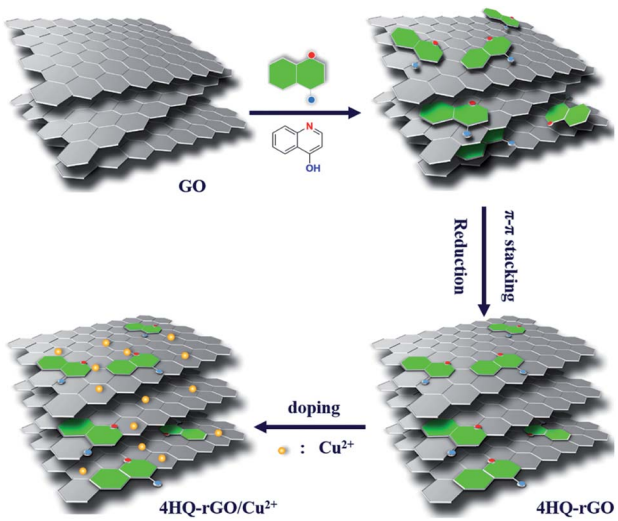

Fig. 1 A typical schematic to prepare the 4HQ-rGO/Cu^{2+} supramolecular assembly used for acetic acid gas sensor applications.

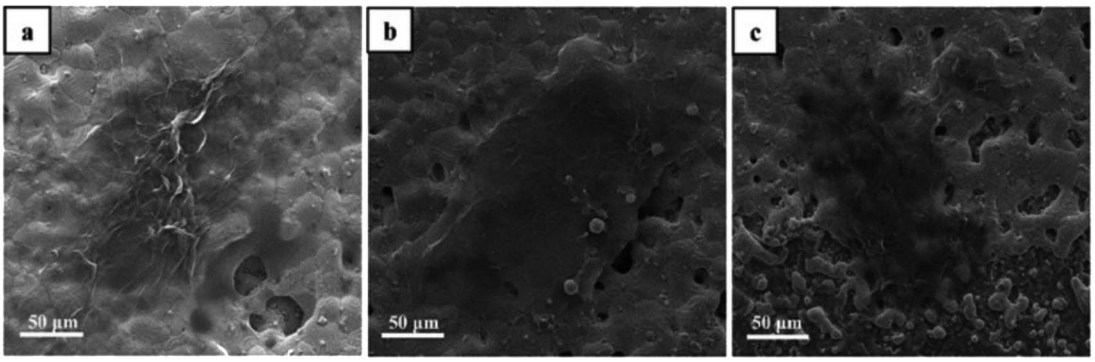

Fig. 2 Typical SEM images of (a) rGO, (b) 4HQ-rGO and (c) 4HQ-rGO/Cu^{2+} deposited on the surface of IDEs used for acetic acid gas sensing.

for the sensor resistance to revert to its initial value. All of the gas-sensing measurements were performed at room temperature (25 °C) with a relative humidity (RH) in the range of 45–65%.

3. Results and discussion

The synthesis process for 4HQ-rGO/Cu^{2+} is systematically presented in Fig. 1. First, a dipolar molecule with a D–π–A structure, 4HQ, was dispersed in the aqueous suspension of GO. After a chemical reduction with hydrazine, most of the oxygen-containing functional groups on the GO nanosheets were removed. Moreover, the 4HQ molecules were attached to the reduced graphene oxide (rGO) nanosheets *via* a supramolecular assembly driven by strong π–π stacking interactions between the 4HQ molecules and the graphene nanosheets. Owing to the hydrophilic –OH group of 4HQ, the 4HQ molecule-doped rGO possessed an exceptional dispersibility in water. Then, the copper(II) ions (Cu^{2+}) were introduced into the 4HQ-rGO composite by directly adding the $CuCl_2$ solution into the 4HQ-rGO suspension. Negatively charged graphene sheets were effectively assembled with positively charged Cu^{2+} due to the electrostatic adsorption.[28,29]

Fig. 2 shows the representative SEM inspections of rGO, 4HQ-rGO, and 4HQ-rGO/Cu^{2+} deposited on the interdigitated electrodes (IDEs). It was observed that the wrinkled rGO nanosheets were seriously aggregated and restacked together on the IDEs (Fig. 2a), resulting in the loss of the interlaminar surface area and finally a largely reduced gas response.[30] While 4HQ-rGO uniformly deposited on the IDEs (Fig. 2b) due to its excellent dispersibility in water,[31] a higher specific surface area and better sensing performance were generated. After the addition of the Cu^{2+} solution ($CuCl_2$, 100 mg mL^{-1}, 0.1–1.0 mL), no obvious morphology change for 4HQ-rGO was found.

The changes in the chemical functional groups of as-prepared 4HQ-rGO can be observed through the Fourier transform infrared (FT-IR) spectrum. As demonstrated in Fig. 3a, two characteristic bands at ~3407 cm^{-1} and ~1722 cm^{-1} in the GO spectra were ascribed to the hydroxy (O–H) stretching vibrations and the carboxyl (C=O) stretching vibrations of the carboxyl group of GO, respectively. A significant decrease in these two peaks in the rGO spectra reveals the successful reduction of graphene oxide. Furthermore, the observed spectrum of 4HQ-rGO shows the –OH stretching vibration at 2919 cm^{-1}. Three characteristic peaks at 1595 cm^{-1}, 1473 cm^{-1}, and 1061 cm^{-1} are attributed ν(C=C), ν(C_5H_5N), and ν(C–OH), respectively. The presence of these peaks in the FT-IR spectrum clearly confirmed the successful assembling of the 4HQ molecules onto the GO nanosheets.

The structural properties of the as-obtained materials were analyzed by Raman scattering spectroscopy. Two sharp peaks at 1334 cm^{-1} and 1592 cm^{-1} are attributed to the D-band and G-

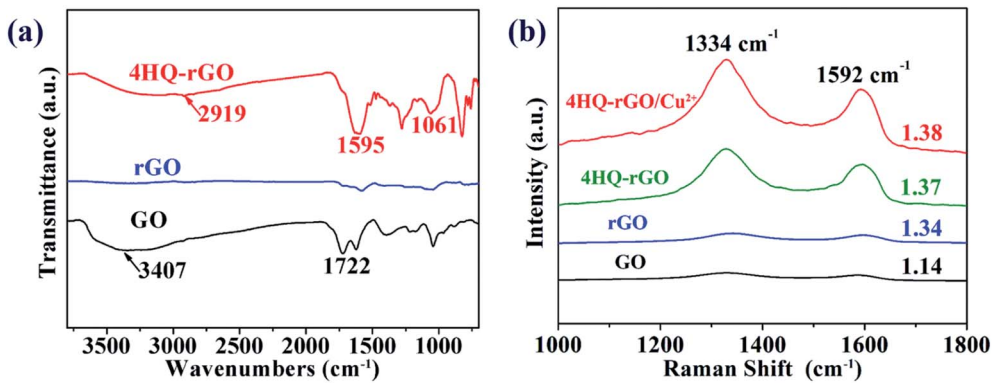

Fig. 3 (a) FT-IR spectra of the GO, rGO, and 4HQ-rGO material. (b) Raman spectra of the GO, rGO, 4HQ-rGO, and 4HQ-rGO/Cu^{2+} material.

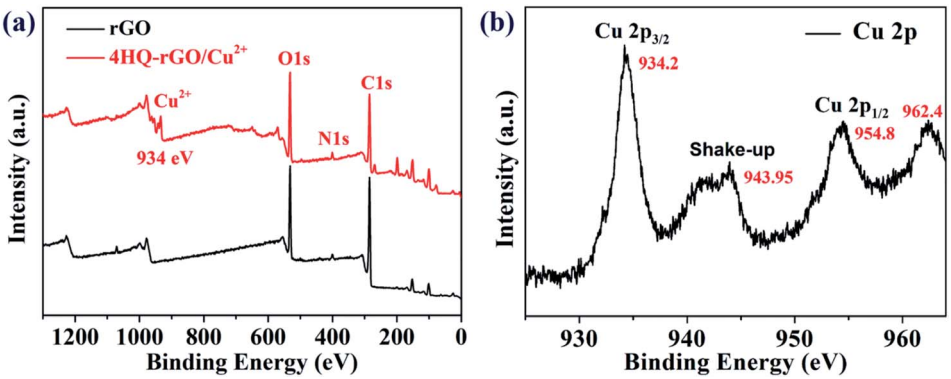

Fig. 4 (a) XPS spectra of the rGO and 4HQ-rGO/Cu^{2+} materials. (b) Typical XPS survey scan spectrum of Cu 2p.

band of all four samples (Fig. 3b).[32] It was clear that the I_D/I_G value for rGO (1.34), 4HQ-rGO (1.37), along with 4HQ-rGO/Cu^{2+} (1.38) were higher than that of GO (1.14), indicating that a new sp^2 cluster appeared after reduction,[33] which also verified the effective reduction with hydrazine hydrate.

Furthermore, the as-prepared rGO and 4HQ-rGO/Cu^{2+} composites were examined by X-ray photoelectron spectroscopy (XPS) (Fig. 4a). The typical peaks for N 1s appeared at 400 eV and Cu^{2+} at 934 eV in the XPS spectrum of 4HQ-rGO/Cu^{2+}, which distinctly proved that the functional 4HQ molecules and Cu^{2+} ions were successfully assembled on the rGO nanosheets. Moreover, Fig. 4b shows the typical XPS survey scan spectrum of Cu 2p, which clearly revealed that the binding energies of Cu $2p_{3/2}$ and Cu $2p_{1/2}$ were located at 934.2 eV and 954.8 eV, respectively.[34] The presence of Cu^{2+} was confirmed by two raised characteristic peaks at 943.95 and 962.4 eV.[35] Compared to the

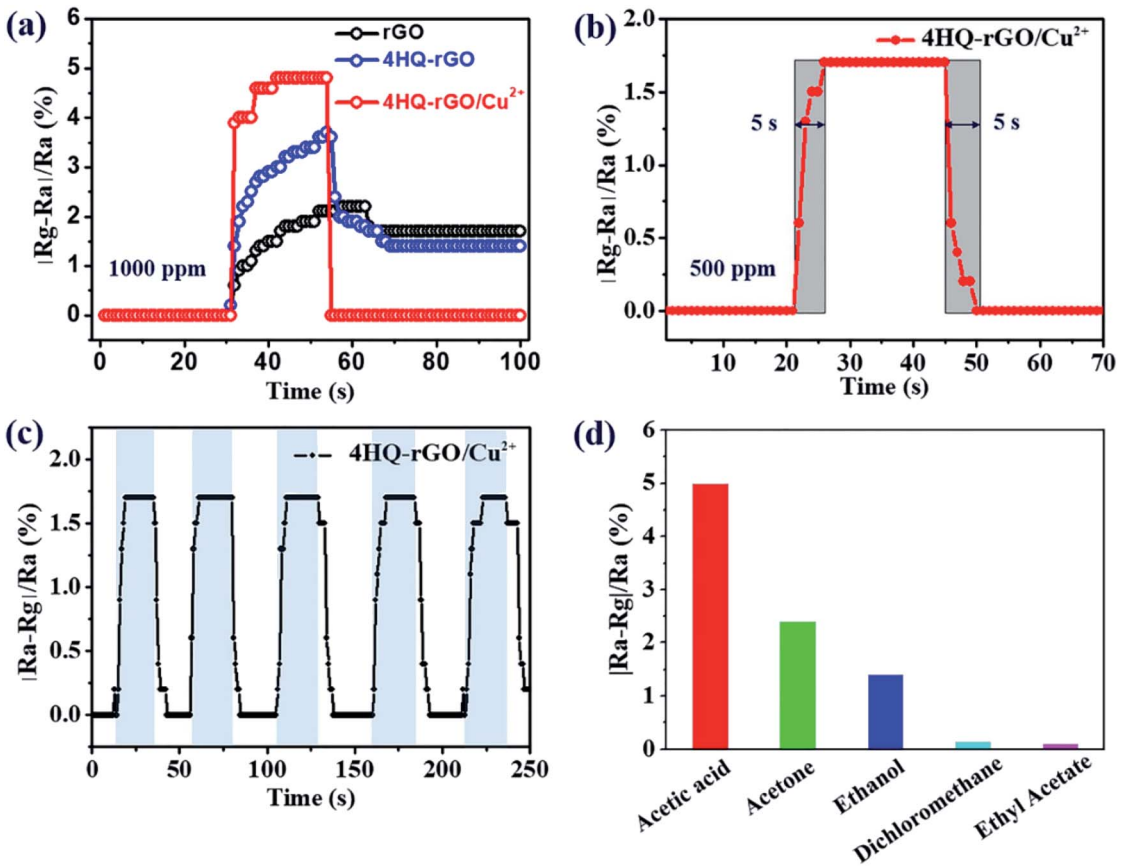

Fig. 5 (a) The typical gas sensing responses for rGO, 4HQ-rGO, and 4HQ-rGO/Cu^{2+} toward 1000 ppm acetic acid at room-temperature. (b) Response and recovery time of the 4HQ-rGO/Cu^{2+} sensing composite upon exposure to 500 ppm acetic acid. (c) Reproducibility of the 4HQ-rGO/Cu^{2+} sensing composite for five successive cycles upon exposure to 500 ppm acetic acid. (d) Selective response of the 4HQ-rGO/Cu^{2+} based sensor toward 1000 ppm acetic acid, acetone, ethanol, dichloromethane, and ethyl acetate.

XPS spectrum of rGO, no other peaks for oxygen were observed in the survey of 4HQ-rGO/Cu^{2+}, which meant that Cu was doped in its ionic form rather than copper oxide.

To measure the composition content in the final samples, the thermal behaviors of 4HQ-rGO and 4HQ-rGO/Cu^{2+} were investigated using a thermal gravimetric analyzer (TGA). As shown in Fig. S3,† the 27 wt% weight loss before 250 °C was related to the decomposition of the 4HQ molecules in the survey for 4HQ-rGO. Therefore, the rGO content was 73 wt%. The lower weight loss of ~5 wt% in the survey for 4HQ-rGO/Cu^{2+} corresponded to the addition of Cu^{2+}. As a result, the rGO content in the 4HQ-rGO/Cu^{2+} composites was calculated to be 59 wt% according to the 4HQ molecule content (22 wt%). The content of the three compositions (*i.e.*, 4HQ, rGO, and Cu^{2+}) in the final samples was approximately 22 wt%, 59 wt%, and 19 wt%, respectively, based on the TGA results.

Using detailed compositional, structural and morphological characterizations, the successful assembly of the 4HQ molecules and Cu^{2+} ions with rGO nanosheets was confirmed. Thus, to explore the effect of the modification on the performance of the acetic acid sensing, the gas sensing performance of the as-prepared materials were examined in an ambient environment. The typical gas sensing response ($|R_a - R_g|/R_a \times 100\%$, where R_a and R_g are the resistances of the sensing material recorded in air and the acetic acid atmosphere, respectively) for rGO, 4HQ-rGO, and 4HQ-rGO/Cu^{2+} are shown in Fig. 5a. It was illustrated that the responses increased when the as-prepared materials were exposed to 1000 ppm acetic acid from the air and the responses decreased back when exposed to air atmosphere. As we expected, 4HQ-rGO exhibited a higher response, which was ascribed to the supramolecular assembly of rGO with the dipolar molecule, 4HQ. As reported,[36,37] the D–π–A structure of 4HQ accelerated the electronic transportation between graphene and acetic acid molecules. Moreover, the introduction of the Cu^{2+} ions further improved the gas sensitivity and dramatically shortened the response and recovery times since the electron-deficient Cu^{2+} promoted the charge transfer between the small molecules and graphene nanosheets.[38] It is worth noting that after switching back to the air atmosphere, the resistance for 4HQ-rGO/Cu^{2+} was perfectly reverted to the initial value, unlike rGO or 4HQ-rGO, which was due to the low-temperature catalytic activity of the copper(II) ions.[39]

To further investigate the influence of the gas concentration on the response and recovery time, the 4HQ-rGO/Cu^{2+} composite was also explored toward sensing 500 ppm acetic acid. It was demonstrated that the sensor exhibited an unique ultra-fast response–recovery characteristic toward 500 ppm acetic acid (initial resistance: 94 740 Ω, 25 °C, RH: 45%). Both the average response and recovery times were within 5 seconds (Fig. 5b).

As stated before, sensors are required to have a high stability and selectivity in practical applications. In order to substantiate the reproducibility and stability of the prepared sensing materials, the 4HQ-rGO/Cu^{2+} based sensors were exposed to 500 ppm acetic acid to achieve five successive response and recovery cycles (Fig. 5c). For the selectivity measurement, 1000 ppm of various gases (*i.e.*, acetic acid, acetone, ethanol, dichloromethane, and ethyl acetate) were chosen to examine the sensing selectivity of 4HQ-rGO/Cu^{2+} at room temperature. As illustrated in Fig. 5d, the 4HQ-rGO/Cu^{2+} based sensors exhibited a high sensing selectivity toward acetic acid. The excellent sensitivity and improved selectivity of the 4HQ-rGO/Cu^{2+} based sensors toward acetic acid could be explained by the band theory.[43,44] The oxygen molecules were absorbed onto the surface of the graphene sheets after exposure to air atmosphere. The absorbed molecules then captured electrons from the conduction band of the graphene sheets to create an electron depletion layer (O_2^- or O^-).[45,46] When transferred into acetic acid, the acetic acid molecules were oxidized by the oxygen species and the electrons captured by oxygen were thereby released to the conduction band of the graphene sheets,[47,48] resulting in a lower resistance state for the sensor.

To further explore the effect of Cu^{2+} on the sensing properties of the 4HQ-rGO/Cu^{2+} composites, control experiments were performed with the assembly of different Cu^{2+} ion content and various transition metal ions that were adjacent to copper in the periodic table of elements (*i.e.*, Mn^{2+}, Fe^{3+}, Co^{2+}, Ni^{2+}, Cu^{2+}, and Cd^{2+}). Compared with 4HQ-rGO, the response for the resultant 4HQ-rGO/Cu^{2+} suspension with a Cu^{2+} concentration of 5 mg mL^{-1} toward 1000 ppm acetic acid increased to 5.0% from 2.8% at room temperature, and the response and recovery times were

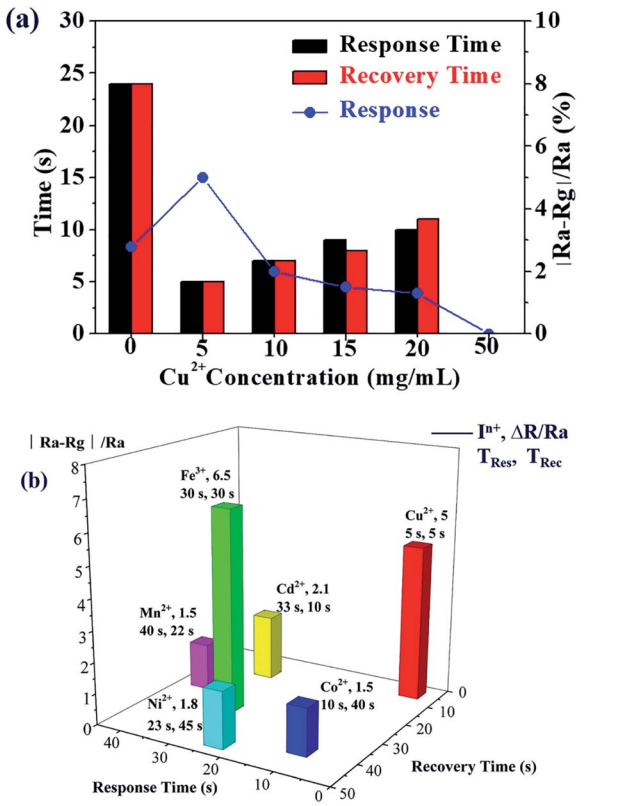

Fig. 6 (a) Typical gas sensing for the 4HQ-rGO/Cu^{2+} composite-based sensors toward 1000 ppm acetic acid at different Cu^{2+} concentrations. (b) The average acetic acid gas sensing responses for the 4HQ-rGO sensing composite doped with copper(II) ions and other metal ions that were adjacent to copper in the periodic table of elements (*i.e.*, Mn^{2+}, Fe^{3+}, Co^{2+}, Ni^{2+}, Cu^{2+}, Cd^{2+}, respectively). ($\Delta R = |R_a - R_g|$, T_{Res}: response time, and T_{Rec}: recovery time).

Table 1 Comparison of the acetic acid gas sensing response and recovery time for typical sensors

Materials & structure	Acetic acid (ppm)	Operating temperature	Response time
Mg-doped ZnO/rGO[21]	100	250 °C	66 s
Nanosized ZnO particles[22]	~300	300 °C	~100 s
Mg-doped ZnO[40]	200	300 °C	145 s
Porous flower-like SnO_2 [41]	500	340 °C	11 s
Coral-like and Y-doped SnO_2 [42]	500	300 °C	7 s
4HQ-rGO/Cu^{2+} (this work)	500	Room temperature	5 s

shortened to 5 s from 24 s, respectively. However, the response value and the response and recovery times both decreased after the further increase in the Cu^{2+} ion content. When the concentration of Cu^{2+} in the $CuCl_2$ solution increased to 50 mg mL^{-1}, the prepared composites even showed no response toward 1000 ppm acetic acid (Fig. 6a).

It is demonstrated in Fig. 6b that the average acetic acid gas sensing responses (R) for 4HQ-rGO assembled with various transition metal ions, *i.e.*, Mn^{2+}, Fe^{3+}, Co^{2+}, Ni^{2+}, Cu^{2+}, and Cd^{2+} (0.5 mL, 5 mg mL^{-1}) were obtained. It was obvious that the composite with the addition of 5 mg mL^{-1} of Cu^{2+} ions had the best sensing performance toward 1000 ppm acetic acid ($R = 5$, $T_{Res} = 5$ s, and $T_{Rec} = 5$ s) at room temperature (Fig. 6b). On one hand, it was proposed that the electron density of the copper(II) ions, which could be modulated by a mild electron-donating effect from adjacent copper ions and the nitrogen dopants of graphene, possessed an electro-catalytic activity to accelerate the gas adsorption rate.[25] On the other hand, the density of the surface π-electrons of the graphene nanosheets were significantly increased due to the electron-rich and electron-deficient atom, which was in accordance with the D–π–A structure for the 4HQ molecules. Therefore, the charge transfer from graphene to the 4HQ molecules was greatly enhanced.

The comparison of the typical acetic acid gas sensors in reported works is summarized in Table 1. It is noteworthy that only the as-prepared 4HQ-rGO/Cu^{2+} composite in this work exhibited the shortest gas response time (within 5 s) at room temperature, which makes it more promising as a room temperature acetic acid gas sensor in practical applications.

4. Conclusions

In summary, a graphene based composite 4HQ-rGO/Cu^{2+} was prepared *via* the supramolecular assembly of graphene nanosheets with 4-hydroxyquinoline (4HQ) and copper(II) ions, which showed enhanced acetic acid sensing properties at room temperature. The 4HQ D–π–A molecules accelerated the charge transfer between the graphene nanosheets and the 4HQ molecules when acetic acid was attached, which is in accordance with the improved sensing properties. Moreover, the copper(II) ions also played a critical role in the main active sites during the process of adsorbing gas molecules at room temperature. The gas sensing measurement revealed that the obtained sensor possessed a high response, outstanding selectivity, and fast response–recovery time (within 5 s). We believe that this study provides a promising approach to developing a high-performance acetic acid gas sensor at room temperature for applications in industry and daily life.

Conflicts of interest

The authors declare no competing financial interest.

Acknowledgements

This work was supported by the National Natural Science Foundation of China (Grant No. 51973070, No. 51673007, and No. 51773069), the Major Project of the Education Bureau of Guangdong Province, the Innovative Team Project of the Education Bureau of Guangdong Province, the Startup Foundation from SCNU, the Guangdong Provincial Key Laboratory of Optical Information Materials and Technology (Grant No. 2017B030301007), and the 111 Project. The authors would also like to acknowledge the support from the Ministry of Education, Kingdom of Saudi Arabia for this research through a grant (PCSED-004-18) under the Promising Centre for Sensors and Electronic Devices (PCSED) at Najran University, Kingdom of Saudi Arabia.

References

1 K. Khojier, *Int. J. Nano Dimens.*, 2017, **8**, 164–170.
2 Y. Tao, X. Cao, Y. Peng, Y. Liu and R. Zhang, *Microchim. Acta*, 2012, **176**, 485–491.
3 F. Wang, H. Li, Z. Yuan, Y. Sun, F. Chang, H. Deng, L. Xie and H. Li, *RSC Adv.*, 2016, **6**, 79343–79349.
4 S. Liu, Z. Y. Wang, J. Zhang, J. Li and T. Zhang, *Sens. Actuators, B*, 2016, **228**, 134–143.
5 J. Wei, B. Liang, Q. Cao, C. Mo, Y. Zheng and X. Ye, *RSC Adv.*, 2017, **7**, 33510.
6 S. Liu, Z. Wang, Y. Zhang, C. Zhang and T. Zhang, *Sens. Actuators, B*, 2015, **211**, 318–324.
7 T. T. Tung, M. J. Nine, M. Krebsz, T. Pasinszki, C. J. Coghlan, D. N. H. Tran, *et al.*, *Adv. Funct. Mater.*, 2017, **27**, 1702891.
8 Z. Wang, T. Han, T. Fei, S. Liu and T. Zhang, *ACS Appl. Mater. Interfaces*, 2018, **10**, 41773–41783.
9 J. Wu, S. Feng, X. Wei, J. Shen, W. Lu, H. Shi, *et al.*, *Adv. Funct. Mater.*, 2016, **26**, 7462–7469.
10 D. Zhang, J. Tong and B. Xia, *Sens. Actuators, B*, 2014, **197**, 66–72.

11 D. Zhang, D. Wang, P. Li, X. Zong and G. Dong, *Sens. Actuators, B*, 2018, **255**, 1869–1877.
12 Z. Song, Z. Wei, B. Wang, Z. Luo, S. Xu, W. Zhang, *et al.*, *Chem. Mater.*, 2016, **28**, 1205–1212.
13 D. Zhang, H. Chang, P. Li, R. Liu and Q. Xue, *Sens. Actuators, B*, 2016, **225**, 233–240.
14 Z. Chen, A. Umar, S. Wang, Y. Wang, T. Tian, Y. Shang, *et al.*, *Nanoscale*, 2015, **7**, 10259–10266.
15 W. Pei, T. Zhang, Y. Wang, Z. Chen, A. Umar, H. Li, *et al.*, *Nanoscale*, 2017, **9**, 16273–16280.
16 Z. Chen, J. Wang, D. Pan, Y. Wang, R. Noetzel, H. Li, *et al.*, *ACS Nano*, 2018, **12**, 2521–2530.
17 S. Wang, Z. Chen, A. Umar, Y. Wang, T. Tian, Y. Shang, *et al.*, *J. Phys. Chem. C*, 2015, **119**, 28640–28647.
18 S. Nag, L. Duarte, E. Bertrand, V. Celton, M. Castro, V. Choudhary, *et al.*, *J. Mater. Chem. B*, 2014, **2**, 6571–6579.
19 X. Chu, P. Dai, Y. Dong, W. Sun, L. Bai and W. Zhang, *J. Mater. Sci.: Mater. Electron.*, 2017, **28**(24), 19164–19173.
20 J. Praneerad, N. Thongsai, P. Supchocksoonthorn, S. Kladsomboon and P. Paoprasert, *Spectrochim. Acta, Part A*, 2019, **211**, 59–70.
21 V. Khorramshahi, J. Karamdel and R. Yousefi, *Ceram. Int.*, 2019, **45**, 7034–7043.
22 T. Prakash, R. Jayaprakash, D. Sathya Raj, S. Kumar, N. Donato, *et al.*, *Sens. Actuators, B*, 2013, **176**, 560–568.
23 D. Li, X. Zeng, Y. Yang, J. Yang and W. Yuan, *Mater. Lett.*, 2012, **74**, 19–21.
24 X. Wang, H. Zhang, H. Lin, S. Gupta, C. Wang, Z. Tao, *et al.*, *Nano Energy*, 2016, **25**, 110–119.
25 L. Chen, J. Li and M. Ge, *J. Phys. Chem. C*, 2009, **113**, 21177–21184.
26 K. Yan and A. Chen, *Energy*, 2013, **58**, 357–363.
27 J. Wang, K. Wang, F.-B. Wang and X.-H. Xia, *Nat. Commun.*, 2014, **5**, 5285.
28 G. Yu, P. Wei, F. Wang and J. Liu, *ChemElectroChem*, 2017, **4**, 1509–1515.
29 J. Wang, T. Wang, F. Wang, D. Zhang, K. Wang and X. Xia, *J. Phys. Chem. C*, 2016, **120**, 15593–15599.
30 Z. Chen, J. Wang, A. Umar, Y. Wang, H. Li and G. Zhou, *ACS Appl. Mater. Interfaces*, 2017, **9**, 11819–11827.
31 R. Jia, P. Xie, Y. Feng, Z. Chen, A. Umar and Y. Wang, *Appl. Surf. Sci.*, 2018, **440**, 409–414.
32 K. N. Kudin, B. Ozbas, H. C. Schniepp, R. K. Prud'homme, I. A. Aksay and R. Car, *Nano Lett.*, 2008, **8**, 36–41.
33 S. Stankovich, D. A. Dikin, R. D. Piner, K. A. Kohlhaas, A. Kleinhammes, Y. Jia, *et al.*, *Carbon*, 2007, **45**, 1558–1565.
34 R. P. Vasquez, *Surf. Sci. Spectra*, 1998, **5**, 262–266.
35 S.-l. Gao, M. Yu, J.-h. Liu, B. Xue and S.-m. Li, *Int. J. Miner., Metall. Mater.*, 2017, **24**, 423–431.
36 O. Canbin, X. Li and A. Cao, *Mater. Lett.*, 2015, **161**, 193–196.
37 A. L. Capodilupo, E. Fabiano, L. De Marco, G. Ciccarella, G. Gigli, C. Martinelli, *et al.*, *J. Org. Chem.*, 2016, **81**, 3235–3245.
38 K. Yan, J. Liao, X. Wu and X. Xie, *RSC Adv.*, 2013, **3**, 3853–3856.
39 J. Wang, T.-T. Wang, F.-B. Wang, D.-Y. Zhang, K. Wang and X.-H. Xia, *J. Phys. Chem. C*, 2016, **120**, 15593–15599.
40 V. Khorramshahi, J. Karamdel and R. Yousefi, *J. Mater. Sci.: Mater. Electron.*, 2018, **29**, 14679–14688.
41 T. Wang, S. Ma, L. Cheng, X. Xu, J. Luo, *et al.*, *Mater. Lett.*, 2015, **142**, 141–144.
42 L. Cheng, S. Ma, T. Wang, J. Luo, X. Li, *et al.*, *Mater. Lett.*, 2014, **137**, 265–268.
43 J. Zhang, F. Liao, Y. Zhu, J. Sun and M. Shao, *Sens. Actuators, B*, 2015, **215**, 497–503.
44 V. Khorramshahi, J. Karamdel and R. Yousefi, *Ceram. Int.*, 2019, **45**, 7034–7704.
45 S. Liu, F. Hu, J. Zhang, H. Tang and M. Shao, *ACS Appl. Mater. Interfaces*, 2013, **5**, 3208–3211.
46 L. Cheng, S. Ma, X. Li, J. Luo, W. Li, F. Li, Y. Mao, T. Wang and Y. Li, *Sens. Actuators, B*, 2014, **200**, 181–190.
47 X. Li, Q. Zhang, S. Ma, G. Wan, F. Li and X. Xu, *Sens. Actuators, B*, 2014, **195**, 526–533.
48 C. Wang, S. Ma, A. Sun, R. Qin, F. Yang, X. Li, F. Li and X. Yang, *Sens. Actuators, B*, 2014, **193**, 326–333.